Two–photon contributions to the Rosenbluth cross–section in the Skyrme model

M. Kuhn and H. Weigel

Fachbereich Physik, Siegen University, D–57068 Siegen, Germany

We study two–photon contributions to the elastic electron nucleon scattering within the Skyrme model. In particular we focus on the role of the anomaly that enters via the Wess–Zumino term and explain how this induces an axial current interaction.

I. INTRODUCTION

Since decades the so–called Rosenbluth separation has been utilized to extract the electromagnetic form factors of the nucleon from the differential cross section for unpolarized electron nucleon scattering. More recently, polarization measurements have become available that provide additional information on these form factors. Surprisingly, substantial inconsistencies between these two measurements of the same physical quantity seem to emerge.

To start discussing the problem we introduce the relevant Lorentz invariant kinematical variables. First we have

$$\tau = \frac{Q^2}{4M^2} = -\frac{q^2}{4M^2} \tag{1.1}$$

where $q = k - k' = p' - p$ is the momentum transfer and M the nucleon mass. For space–like processes, such as the elastic electron nucleon scattering, $Q^2 = -q^2$ is non–negative. The second Lorentz invariant variable is the photon polarization parameter

$$\epsilon = \frac{\nu^2 - M^4 \tau (1 + \tau)}{\nu^2 + M^4 \tau (1 + \tau)} \qquad \text{where} \qquad \nu = \frac{1}{4} (k + k') \cdot (p + p') . \tag{1.2}$$

The leading (tree level) contribution to elastic electron nucleon scattering is shown as Feynman diagram in figure 1. In this one–photon exchange (or Born) approximation the unpolarized elastic electron nucleon scattering cross section is

$$\frac{d\sigma}{d\Omega} = \left(\frac{d\sigma}{d\Omega}\right)_{\text{Mott}} \frac{\epsilon\, G_E^2(Q^2) + \tau\, G_M^2(Q^2)}{\epsilon(1 + \tau)} \tag{1.3}$$

in the limit of vanishing electron mass, $m_e \to 0$, which is well justified in the considered kinematical regime. In eq. (1.3) $G_{E,M}$ are the electromagnetic form factors of the nucleon to be further specified later. The Rosenbluth separation to extract these form factors from data is to display the ratio of the measured cross section and the Mott cross section at a given momentum transfer, *i.e.* τ as function of ϵ. After multiplicating this function with $\epsilon(1 + \tau)$, the intercept and slope yield G_M and G_E, respectively.

However, since the relative contribution of G_E to the cross section quickly decreases with growing momentum transfer, this type of analysis becomes increasingly difficult already
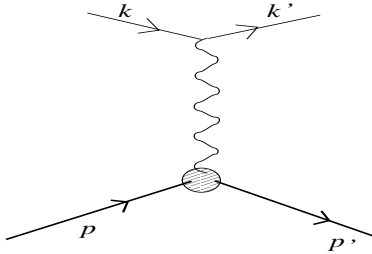
FIG. 1: Tree level loop contribution to the electron (momenta k and k') nucleon momenta p and p') scattering with a local nucleon two–photon vertex.

at $Q^2 \sim 1\text{GeV}^2$. Yet the results of this separation have turned out consistent with the assumption that the ratio

$$R(Q^2) = \frac{\mu_p G_E(Q^2)}{G_M(Q^2)} \,, \tag{1.4}$$

where $\mu_p = G_M(0)$ is the proton magnetic moment, approximately equals unity [1]. More recently, it has become possible to directly extract this ratio from polarization observables [2], thereby avoiding the potentially uncertain separation technique. Most surprisingly, these direct measurements exhibited a linear fall

$$R(Q^2) \approx 1 - 0.13 \left(Q^2[\text{GeV}]^2 - 0.04\right) \tag{1.5}$$

indicating an eventual root at about $Q^2 \sim 10\text{GeV}^2$. Such a behavior was already suggested as early as 1973 [3] within semi–empirical fits to existing data. More recently this structure has been predicted within a chiral soliton model study [4]. To resolve this puzzle, the Rosenbluth separation has been repeated with significantly improved precision [5]. For this technique to be operative, it is important that the data are indeed consistent with this linear relation [6]. Not only is this indeed the case but also the previous result $R \approx 1$ is reproduced. Hence we face the paradox situation that two distinct methods to experimentally determine a fundamental nucleon property yield inconsistent results [7].

A possible resolution could be that contributions to the cross section that stem from two–photon exchanges but have been omitted so far, are amplified with increasing Q^2. In turn, the Rosenbluth separation yields modified form factors that significantly deviate from the ones that are defined via a one photon exchange [8]. On the other hand, symmetry properties require that the two–photon exchange contributions alter the (linear) dependence on the photon polarization parameter ϵ [9]. Yet the data are consistent with but not restricted to this linear dependence [10]. It is widely believed [11] that the two–photon mainly effects the Rosenbluth method but are negligibly small for the polarization process. We will therefore focus on the former.

There are two types of two–photon exchange Feynman diagrams that we display in figures 2 and 3. The box diagrams in figure 2 are essentially iterations of the one–photon exchange shown in figure 1. Any estimate of these box diagrams require additional information about the off–shell behavior of the photon–nucleon vertex. Furthermore the intermediate baryon is not restricted to be the nucleon, it could be any nucleon resonance that possesses a sizable electro–production potential. Many assumptions and modeling of baryon properties enter the computation of these diagrams [8, 12, 13, 14, 15]. For a recent review on both the experimental and the theoretical situations see ref. [11, 16].
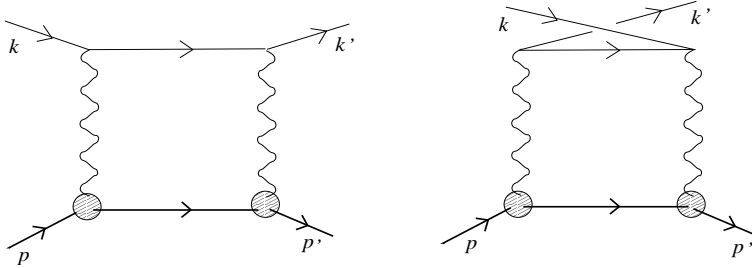
FIG. 2: One loop contribution to the electron (momenta k and k') nucleon (momenta p and p') scattering within a typical box diagram. In the hadronic picture, the intermediate baryon can be any nucleon resonance [15], while in the quark picture the photon nucleon vertex can, *e.g.* be related to generalized parton distributions [11].

The second type of diagrams shown is in figure 3 and has the photon coupled to the nucleon at a single vertex. Such diagrams are curious because they do not appear in simple Dirac theories of the nucleon which are linear in the covariant derivative. Nevertheless, such diagrams are not unknown in hadron physics. In particular, the $\pi^0 \to \gamma\gamma$ decay induces such a vertex as shown in figure 4. In that case the intrinsic structure of the $\pi^0\gamma\gamma$ vertex is dictated by the quark triangle diagram, *i.e.* the axial anomaly. So we may imagine the nucleon coupling to an (off–shell) pion via a Yukawa interaction and the pion subsequently decaying into an electron–positron pair as in figure 4. As we will observe, this process is negligible since (after renormalization) this diagram turns out to vanish in the limit $m_{\mathrm{e}} \to 0$. The reason is that in the interaction Lagrangian the two photons couple to the derivative of the pion field and, when computing the Feynam diagram, an integration by parts produces a factor m_{e}. Hence the single pion exchange cannot produce a significant contribution to electron proton scattering. However, in chiral model multiple pion exchanges cease to have derivative couplings to the two photons and are hence not necessarily suppressed when $m_{\mathrm{e}} \to 0$.

The main purpose of the present investigation is to point out that this anomaly induced process has a considerable affect for two photon contributions in the Rosenbluth analysis and that this process has not been considered previously. Of course, this process by itself cannot fully explain the discrepancy to the polarization analysis.

The required anomaly contribution to the local process shown in figure 3 can be perfectly studied within chiral soliton models for baryons. In these models the chiral field U not only is the non–linear representation of the pion field but also describes the nucleon as a (topological) soliton excitation. In these models we may understand the two–photon exchanges shown in figure 3 as the coupling of the nucleon's pion cloud to the electron through the anomaly. We will particularly compute the diagram in figure 3 within the Skyrme model and focus on the anomaly contribution which is unique because it reflects a QCD property. Diagrams that have two photons coupled to the nucleon at a single vertex are unique to chiral models because they are formulated in meson degrees of freedom. There are also non–anomalous local two–photon couplings. These are quite model dependent. Therefore we will here only consider the one induced by the non–linear σ model as an example and observe that its contribution vanishes as $m_{\mathrm{e}} \to 0$.

The soliton model successfully describes many properties of baryons and baryon resonances. Though quantitatively the agreement with empirical data is on the $\mathcal{O}(1/N_{\mathrm{C}})$, *i.e.* 30%, qualitative aspects are well explained, as has been recently reviewed in ref. [17].
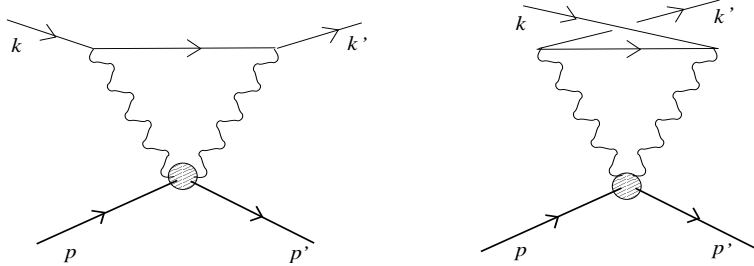
FIG. 3: One loop contribution to the electron (momenta k and k') nucleon (momenta p and p') scattering with a local nucleon two–photon vertex.
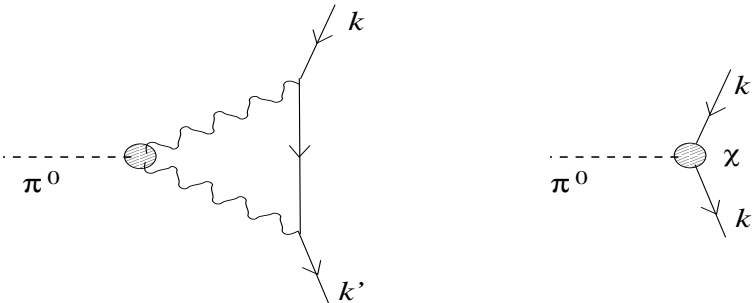

FIG. 4: One loop contribution to the anomalous decay of the neutral pion into a electron positron pair. Left panel: loop diagram from eq. (3.3), right panel: contribution from the local counterterm eq. (3.4). There is an analogous contribution from the loop diagram with the external electron legs exchanged, *cf.* figure 3.

This makes this model a perfect candidate to explore the above posed problem. The use of model calculations is the more unavoidable since in due time lattice calculations for (off–shell) two–photon form factors will not be available. Furthermore we recall that in soliton models two–photon interactions have previously been successfully considered to compute static nucleon polarizabilities [18]. Of course, the current problem goes beyond treating these interactions in a static framework.

II. THE MODEL

We consider the two–flavor Skyrme model for baryons as the simplest of many models that support the soliton picture. In terms of the non–linear representation for the isovector pion field $\vec{\pi}$

$$U = \exp\left[i\frac{\vec{\pi}\cdot\vec{\tau}}{f_\pi}\right] , \qquad (2.1)$$

where $\vec{\tau}$ is the vector of Pauli matrices, this model is defined by the Lagrangian

$$\mathcal{L} = \frac{f_\pi^2}{4}\mathrm{tr}\left(\partial_\mu U\partial^\mu U^\dagger\right) + \frac{1}{32e_{\mathrm{Sk}}^2}\mathrm{tr}\left(\left[\partial_\mu U, \partial_\nu U^\dagger\right]\left[\partial^\mu U, \partial^\nu U^\dagger\right]\right) + \frac{f_\pi^2 m_\pi^2}{4}\mathrm{tr}\left(U + U^\dagger - 2\right) . \quad (2.2)$$

The leading contribution is the non–linear–σ–term, which is supplemented by the Skyrme term which contains four derivatives on the chiral field and is required to eventually stabilize

the soliton. Also the chiral symmetry breaking pion mass term is added. The model parameters that are determined from meson properties are the pion decay constant $f_\pi = 93\text{MeV}$ and the pion mass $m_\pi = 138\text{MeV}$. On the other hand, the Skyrme term coupling $e_{\text{Sk}} \approx 4.0$ may vary within a certain regime imposed by reproducing nucleon static properties reasonably well.

The hedgehog configuration that builds the soliton and carries unit baryon number reads

$$U_0(\vec{r}) = \exp\left[i\vec{\tau} \cdot \hat{r} F(r)\right] \tag{2.3}$$

where $r = |\vec{r}|$. The chiral angle, $F(r)$ is determined from the stationary conditions that result from eq. (2.2) subject to the boundary conditions $F(0) = \pi$ and $F(\infty) = 0$. To generate baryon states with good spin and isospin we subsequently introduce collective coordinates $A \in SU(2)$

$$U(\vec{r}, t) = A(t)U_0(\vec{r})A^\dagger(t) \tag{2.4}$$

that parameterize the spin–flavor orientation of the hedgehog and quantize them canonically. This turns the time variation of the collective coordinates into the spin operator,

$$\vec{J} = \alpha^2[U_0]\,\text{tr}\left[(-i)\vec{\tau}A^\dagger \frac{dA}{dt}\right], \tag{2.5}$$

where the moment of inertia, $\alpha^2[U_0]$ is a functional of the classical hedgehog field. Its invariance under combined spin and isospin rotations yields the isospin operator as

$$I_a = -D_{ab}J_b \qquad \text{with} \qquad D_{ab} = \frac{1}{2}\,\text{tr}\left[\tau_a A\tau_b A^\dagger\right]. \tag{2.6}$$

In this relation D_{ab} refers to the adjoint representation D_{ab} of the collective rotations.

The nucleon wavefunction are Wigner–D functions of the collective coordinates in the spin $J = \frac{1}{2}$ and isospin $I = \frac{1}{2}$ representation

$$\langle A|J = I, t, s\rangle = \left[\frac{2J+1}{8\pi^2}\right]^{1/2} D_{t,s}^{J=I}(A). \tag{2.7}$$

Here $|s, t\rangle$ represents a nucleon state with spin and isospin projections $s = \pm\frac{1}{2}$ and $t = \pm\frac{1}{2}$, respectively. The identification of total spin and isospin originates from the hedgehog structure upon which rotations in coordinate and iso– space are identical.

In practice we obtain operators for observables that are expressed in terms of the collective coordinates and their time derivatives. We use eqs (2.5) and (2.6) to write the latter as operators in the space of the collective coordinates and sandwich them between the wavefunctions eq. (2.7). The matrix elements are finally obtained as integral over the collective coordinates which are most conveniently evaluated in terms of their Euler angle representation. Later we will particularly require

$$\langle s, t|D_{ab}|s', t'\rangle = -\frac{4}{3}\langle s, t|I_a J_b|s', t'\rangle \qquad \text{and} \qquad \langle s, t|D_{3a}D_{3b}|s', t'\rangle = \frac{1}{3}\langle s, t|\delta_{ab}|s', t'\rangle. \tag{2.8}$$

These results and techniques are well established in soliton models and we refer to reviews, e.g. [17], for derivation and further details. These collective coordinate matrix elements come together with the matrix elements that emerge from the spatial dependence of the soliton. We will return to their computation in section IV.

III. ONE AND TWO–PHOTON INTERACTIONS

We obtain the minimal photon Skyrmion interaction by gauging the Lagrangian. Later we will also comment on non–minimal interactions. For the local part, eq. (2.2) this is straightforwardly accomplished by replacing the partial derivatives with covariant ones:

$$\partial_\mu U \longrightarrow D_\mu U = \partial_\mu U - ieA_\mu \left[\hat{Q}, U\right] . \tag{3.1}$$

Here $\hat{Q} = \tau_3/2 + \mathbb{1}/6$ and A_μ are the quark charge matrix and the photon field, respectively. Substituting this prescription not only yields the single photon vertex to the nucleon (represented by the soliton) but also higher order interactions, in particular two–photon vertices, the so–called seagull terms. For example, the non–linear–σ–term in eq. (2.2) gives

$$\begin{aligned}
\mathcal{L}_{\text{nl}\sigma}^{\text{(gauged)}} &= \frac{f_\pi^2}{4}\text{tr}\left(\partial_\mu U \partial^\mu U^\dagger\right) - i\frac{f_\pi^2 e}{2}A_\mu \text{tr}\left(\hat{Q}\left[U^\dagger \partial^\mu U + U\partial^\mu U^\dagger\right]\right) \\
&\quad -\frac{f_\pi^2 e^2}{4}A_\mu A^\mu \, \text{tr}\left(\left[\hat{Q}, U\right]\left[\hat{Q}, U^\dagger\right]\right) .
\end{aligned} \tag{3.2}$$

The situation is slightly more complicated for the non–local Wess–Zumino term [19] that we do not make explicit because it does not contribute to pure hadronic objects in the two–flavor Skyrme model. This term encodes the QCD anomaly and yields one and two–photon couplings to the chiral field when gauged with respect to the corresponding $U(1)$ group. The techniques to compute these couplings are based on a trial and error scenario to obtain a gauge invariant quantity. These techniques are widely described in the literature [19, 20] and the result for the gauged Lagrangian is

$$\begin{aligned}
\mathcal{L}_{\text{WZ}}^{\text{gauged}} &= \frac{e}{16\pi^2}\epsilon^{\mu\nu\rho\sigma}\Big\{A_\mu \text{tr}\left(\hat{Q}\left[U^\dagger \partial_\nu U U^\dagger \partial_\rho U U^\dagger \partial_\sigma U - U\partial_\nu U^\dagger U \partial_\rho U^\dagger U \partial_\sigma U^\dagger\right]\right) \\
&\quad +ieA_\mu \partial_\nu A_\rho \text{tr}\left(2\hat{Q}^2\left[U^\dagger \partial_\sigma U - U\partial_\sigma U^\dagger\right] + \hat{Q}\partial_\sigma U \hat{Q}U^\dagger - \hat{Q}U\hat{Q}\partial_\sigma U^\dagger\right)\Big\},
\end{aligned} \tag{3.3}$$

wherein we substituted the physical value of three color degrees of freedom. Most interestingly this contribution to the action generates a vertex for the neutral pion to anomalously decay into two photons via the expansion $U = 1 + i\vec{\tau} \cdot \vec{\pi}/f_\pi + \ldots$ of eq. (2.1). Taking into account the QED coupling to the electrons, $eA_\mu \overline{\Psi}_e \gamma^\mu \Psi_e$, this then describes the decay $\pi^0 \rightarrow e^+ e^-$ via the Feynman diagram displayed in the left panel of figure 4. This process was exhaustively discussed in ref. [21] together with its generalization to $\eta \rightarrow \mu^+ \mu^-$, etc.. As a matter of fact, this loop diagram is ultra–violet divergent and induces the counterterm

$$\mathcal{L}_{\text{c.t.}} = \frac{i\alpha^2}{32\pi^2}\chi(\Lambda)\overline{\Psi}_e \gamma^\mu \gamma_5 \Psi_e \text{tr}\left(2\hat{Q}^2\left[U^\dagger \partial_\sigma U - U\partial_\sigma U^\dagger\right] + \hat{Q}\partial_\sigma U \hat{Q}U^\dagger - \hat{Q}U\hat{Q}\partial_\sigma U^\dagger\right) , \tag{3.4}$$

where $\alpha = e^2/4\pi = 1/137$ is the QED fine structure constant. Furthermore χ is a divergent coefficient[1] such that the sum of the two diagrams in figure 4 is finite. Furthermore Λ refers to the normalization scale that enters to properly reproduce the dimensions of loop

---

[1] In ref. [21] counterterm coefficients were independently introduced for the terms in eq. (3.4). However, gauge invariance enforces them to appear in exactly the displayed manner.

integrals in dimensional regularization with $\int d^4 l \to \Lambda^{4-D} \int d^D l$. We separate the finite, but renormalization scheme dependent part according to

$$\chi_{\text{fin}}(\Lambda) = 6 \left(\frac{4}{4-D} - \gamma + \ln 4\pi \right) - \chi(\Lambda) , \tag{3.5}$$

where $\gamma = 0.577\ldots$ is Euler's constant. We consider this renormalization as effective modeling of an eventual off–shell form factor for the $\pi^0 \gamma\gamma$ vertex [22]. After all, classically there is no direct interaction as in eq. (3.4) between electrons and hadrons. On the other hand, a vertex form factor that deceases with the photon momentum renders the diagram in figure 4 finite and thus does not induce such a direct (and unphysical) electron pion interaction.

The resulting decay width is most conveniently presented in terms of the ratio with respect to the decay into two real photons,

$$\frac{\Gamma(\pi^0 \to e^+ e^-)}{\Gamma(\pi^0 \to \gamma\gamma)} = \frac{\alpha^2 m_e^2}{8\pi^2 m_\pi^2} \frac{\sqrt{\xi^2 - 1}}{\xi} |A(\xi)|^2 , \tag{3.6}$$

where $\xi = \frac{m_\pi^2}{4 m_e^2}$. The complex amplitude $A(\xi)$ has a complicated representation in terms of Feynman parameter integrals [21]. Here it suffices to remark that the renormalization scale dependence emerges only through its real part,

$$\text{Re}\, A(\xi) = \chi_{\text{fin}}(\Lambda) - 6 \ln \frac{m_\pi^2}{\Lambda^2} - \left[\ln \left(\xi^2 \right) \right]^2 + 2 \left[3 - 2\ln(2) \right] \ln \left(\xi^2 \right) + \widetilde{A}(\xi) \tag{3.7}$$

where the reminder, $\widetilde{A}(\xi)$ is independent of Λ and finite as $m_e \to 0$. In this massless limit the ultra–violet finite imaginary part

$$\text{Im}\, A(\xi) = \frac{4\pi\xi}{\sqrt{\xi^2 - 1}} \ln \left(\xi + \sqrt{\xi^2 - 1} \right) \tag{3.8}$$

also diverges logarithmically.

The empirical datum $(6.3 \pm 0.5) \times 10^{-8}$ [24] for the ratio, eq. (3.6) is reproduced in the range $-24 < \chi_{\text{fin}}(\Lambda) < -10$ when the renormalization scale in the second term on the right hand side of eq. (3.7) is set to $\Lambda = 1\text{GeV}$. We will adopt that range when investigating two–photon processes in the nucleon sector.

A further remark on the limit $m_e \to 0$ is in order. Eventually we want to assume this limit when computing the cross section for electron nucleon scattering since it considerable simplifies the kinematics and, of course, is physically meaningful because the energy scales that are involved in this scattering process are huge compared to the electron mass. Obviously the width, eq. (3.6) vanishes in that limit. This can be easily understood: W_μ is a total derivative in the one pion approximation. When shuffling this derivative to the electron axial current to which the photons in the loop couple, a factor m_e is produced. So this decay goes together with a helicity flip of the electron. Hence our renormalization condition prevents us from taking the limit $m_e \to 0$ in the loop. As can be observed from eq. (3.7) the loop itself actually produces a double–logarithmic divergence [21].

IV. NUCLEON FORM FACTORS

To compute the transition matrix elements for elastic electron nucleon scattering we consider eqs. (3.2) and (3.3) as perturbation and couple the photons to the electrons as

indicated in figures 1 and 3. This procedure is standard in QED. However, we also need to compute the nucleon matrix elements for the rotating hedgehog configuration, eq. (2.4). These matrix elements are commonly parameterized in terms of form factors. If we extract the terms linear in A_μ and write it as $\mathcal{L}^{(1)} = e J_\mu A^\mu$ the corresponding matrix elements introduce Dirac and Pauli form factors via

$$\langle N(\vec{p}')|J_\mu|N(\vec{p})\rangle = \overline{U}(\vec{p}') \left[\gamma_\mu F_1(Q^2) + \frac{i\sigma_{\mu\nu}q^\nu}{2M} F_2(Q^2) \right] U(\vec{p}) , \tag{4.1}$$

where p_μ and p'_μ are the on–shell momenta of the initial and final nucleons and $q_\mu = p'_\mu - p_\mu$ is the momentum transfer. The above definition is the standard Lorentz covariant parameterization of the matrix elements of the conserved electro–magnetic current, in which $U(\vec{p})$ is the nucleon Dirac spinor. Note that M is just a parameter in this decomposition and refers to the actual nucleon mass rather than the model prediction. It is convenient to introduce "electric" and "magnetic" (so called Sachs) form factors

$$G_E(Q^2) = F_1(Q^2) - \frac{Q^2}{4M^2} F_2(Q^2) , \qquad G_M(Q^2) = F_1(Q^2) + F_2(Q^2) , \tag{4.2}$$

that show up in the differential cross section, eq. (1.3). By pure definition the above form factors concern one–photon couplings to the nucleon. Unfortunately, they cannot easily be accessed from data because nature does not terminate at that order of perturbation theory.

Similarly the two–photon couplings that we extract from eqs. (3.2) and (3.3),

$$\mathcal{L}^{(2)}_{\mathrm{nl}\sigma} = e^2 A_\mu A^\mu S \qquad \text{and} \qquad \mathcal{L}^{(2)}_{\mathrm{WZ}} = e^2 \epsilon^{\mu\nu\rho\sigma} A_\mu \partial_\nu A_\rho W_\sigma \tag{4.3}$$

respectively, also define form factors. While there is only a single and simple Lorentz structure for S,

$$\langle N(\vec{p}')|S|N(\vec{p})\rangle = \overline{U}(\vec{p}') S_{\mathrm{nl}\sigma}(Q^2) U(\vec{p}) , \tag{4.4}$$

the anomaly requires W_μ to be an axial vector with the decomposition

$$\langle N(\vec{p}')|W_\mu|N(\vec{p})\rangle = \overline{U}(\vec{p}') \left[\gamma_\mu F_A(Q^2) + q_\mu F_p(Q^2) + i\sigma_{\mu\nu}q^\nu F_E(Q^2) \right] \gamma_5 U(\vec{p}) . \tag{4.5}$$

There is no simplification or relation between these form factors as for the ordinary axial current because no conservation law applies to W_μ. Yet we will see that for unpolarized scattering, that concerns the Rosenbluth method, only the first form factor, F_A contributes.

In the soliton model a major task consists in computing the momentum dependent form factors in eqs. (4.1), (4.4) and (4.5). In principle an additional collective coordinate that parameterizes the position of the soliton must be introduced in eq. (2.4). Its conjugate momentum will be the linear nucleon momentum. This yields quite a simple recipe to handle the linear momentum part of the matrix elements [25]: just take the Fourier transformation with respect to (minus) the momentum transfer of the coordinate dependent factors in the decomposition of the current operators after substituting the soliton configuration. Essentially we will have to fold the radial functions in the currents by spherical Bessel functions associated with angular momentum of the multiply angular structure. In general we may choose any frame to do this calculation. However, it turns out that the Breit frame with

$$\vec{p} = -\vec{p}' = -\frac{\vec{q}}{2} \qquad \text{and} \qquad q^0 = 0 \tag{4.6}$$

is particularly suited not only because it properly reflects the zero energy transfer onto an infinitely heavy (large N_C) soliton but also because it directly connects the electric form factor, G_E and the magnetic form factor, G_M to the time and spatial components of the electro–magnetic current, respectively. In this frame the incoming and outgoing nucleons evidently have the same energy $E = p^0 = p'^0 = \sqrt{M^2 + Q^2/4}$. For baryons with spin $\frac{1}{2}$ we the find the Sachs form factors from the matrix elements

$$\begin{aligned}
\langle N(\vec{p}')|J^0(0)|N(\vec{p})\rangle &= 2MG_E(Q^2)\langle s_3'|s_3\rangle \\
\langle N(\vec{p}')|J^i(0)|N(\vec{p})\rangle &= -2iG_M(Q^2)\epsilon^{ijk}q^j\langle s_3'|S_k|s_3\rangle\,,
\end{aligned} \qquad (4.7)$$

where $\vec{S}$ is the nucleon spin operator.

So far we have treated the model in a non–relativistic fashion that restricts the energy range to be reliably considered below the nucleon mass. Using the techniques and results of refs. [26, 39] we may extend the nucleon form factor calculation to larger momenta by the transformation

$$G_E(Q^2) \longrightarrow \gamma^{-2n_E}G_E\left(\frac{Q^2}{\gamma^2}\right) \qquad \text{and} \qquad G_M(Q^2) \longrightarrow \gamma^{-2n_M}G_M\left(\frac{Q^2}{\gamma^2}\right)\,, \qquad (4.8)$$

where $\gamma = \sqrt{1+\tau}$ is the Lorentz boost factor. Essentially this transforms the from factors from the non–relativistic to a relativistic frame. It is worthwhile to note that operator ordering ambiguities in quantizing the linear momentum are mitigated by choosing the Breit frame as starting point. This is so because we have $\vec{p}^2 = \vec{p}'^2$ for this special frame. The original study [26] is based on the Lorentz boost and suggests to put $n_E = 0$ and $n_M = 1$. For more insight it is instructive to reflect on the nature of the transformation, eq. (4.8). Most evidently the momentum interval $[0, 4M^2]$ of the rest frame is mapped onto the space–like momenta in the Breit frame. While small momenta are almost unaffected, the form factors at infinity in the Breit frame are obtained from those in the rest frame at $Q^2 = 4M^2$. Even though the latter may be small, there is no general reason for them to vanish. In particular, this implies that the form factors do not match the empirical dipole form unless $n_E = n_M \geq 2$. Thus the values $n_E = n_M \geq 2$ are also frequently adopted because they are strongly motivated by regarding the baryon as a cluster of particles whose leading Fock component is a three particle state [40, 41]. In any case, the large Q^2 behavior is not a profound model result but merely originates from the boost prescription and thus mainly reflects the kinematical situation. We will henceforth assume $n_E = n_M = 2$ and similarly $n_{\rm WZ} = 2$ for the form factors in eq. (4.5). We note that there is an additional ambiguity in the choice of the mass parameter in the Lorentz factor γ. We take M to be the nucleon mass, yet from the point of view from an $1/N_C$ expansion one could equally well argue for the soliton mass which is about 50% larger. Again, this does not significantly affect qualitative results.

In figure 5 we show the resulting form factors G_E and G_M and compare them with data. The data for G_M are obtained according to the Rosenbluth method while the ratio G_M/G_E is taken from polarization measurements that are assumed to be more robust against the two–photon contamination. As usual we display these data normalized to the dipole form factor,

$$G_D(Q^2) = \frac{1}{\left(1 + Q^2/0.71\text{GeV}^2\right)^2}\,. \qquad (4.9)$$

This figure clearly demonstrates that soliton models are able to reproduce the gross features of the empirical form factors. This is particularly the case for the linear fall of the ratio
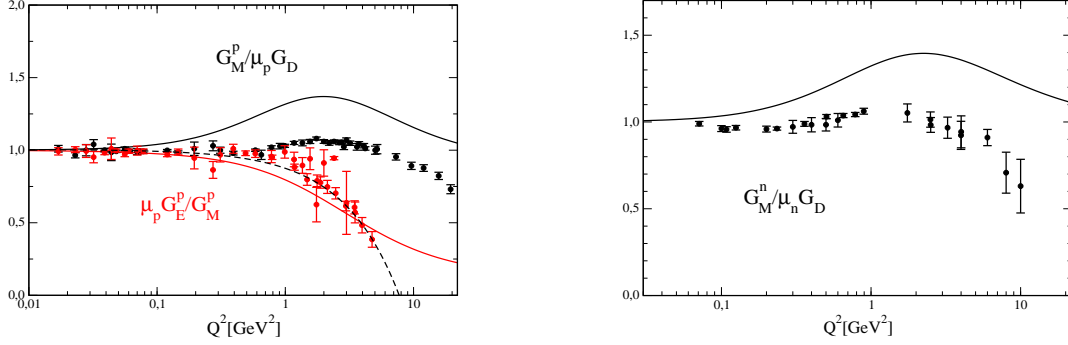
FIG. 5: Proton (left) and neutron (right) form factors computed in the Skyrme model as a function of momentum transfer after applying the boost. These data have been generated with $e_{\rm Sk} = 3.8$. The magnetic from factors are additionally normalized with respect to the predicted magnetic moments $\mu_{\rm p} = G_{\rm M}^{\rm p}(0) \approx 2.33$ and $\mu_{\rm p} = G_{\rm M}^{\rm n}(0) \approx -1.99$. The dashed line represents the empirical fit, eq. (1.5). Data are from refs. [27, 28, 29, 30, 31, 32, 33, 34, 35].
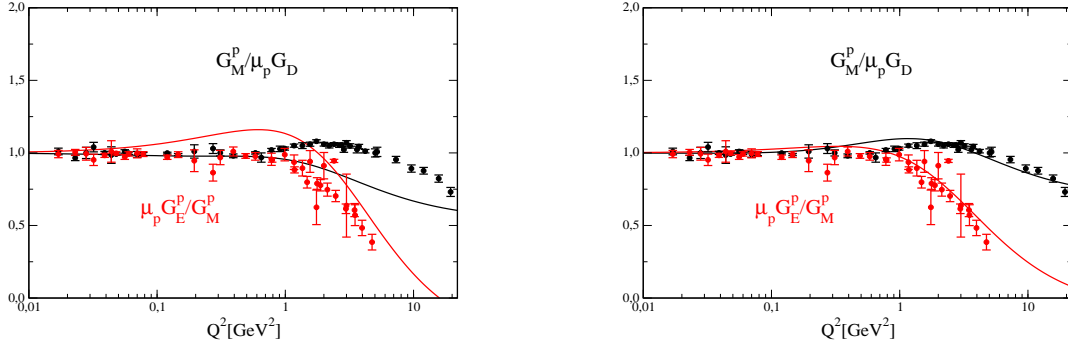

FIG. 6: The influence of the non–minimal photon coupling, eq. (4.10), on the proton form factors for two parameters $L_9 = 0.0069$ (left) and $L_9 = 0.0045$ (right). All other model parameters are as in figure 5.

$R(Q^2)$, *cf.* eqs. (1.4) and (1.5). Taking the point of view, that two–photon corrections are small for the polarization method [11] it is hence our task to explain the Rosenbluth cross section within the model.

Nevertheless, deviations of the model predictions from the actual data are apparent. Model modifications can improve the agreement with data. For example, it is known from chiral perturbation theory studies on the pion radius [36] that non–minimal photon couplings as in

$$\mathcal{L}_9 = -iL_9 A^{\mu\nu}{\rm tr}\left[Q\left(\partial_\mu U \partial_\nu U^\dagger + \partial_\mu U^\dagger \partial_\nu U\right)\right] , \tag{4.10}$$

are mandatory to correctly reproduce the pion electromagnetic properties. In eq. (4.10) $A^{\mu\nu}$ is the photon field strength tensor and $L_9 \approx 0.0069$ is adjusted to the pion radius [37]. This term may be understood as resembling the contribution from (short distance) vector meson fields that have been integrated out when approximating the effective chiral theory by the Skyrme model [38]. In figure 6 we show the proton form factors when the non–minimal electro–magnetic coupling, eq. (4.10), is incorporated in the the electromagnetic current. As can be seen from the right panel of that figure, a moderate adjustment of the additional parameter indeed leads to excellent agreement with data. This is particularly the case for

the linear decay of R. Being a total derivative, eq. (4.10) does not affect the form factors at zero momentum transfer.

The reader may also consult ref. [39] for a more thorough investigation in a vector meson soliton model that strongly supports the above statement that soliton models provide a fair account of the nucleon form factors, even at large momenta. That investigation also shows that the just mentioned deviation from the data can be removed by fine tuning the model. The Lorentz boost, eq. (4.8) is crucial to gain that agreement. As explained in ref. [39] the strong decrease of the ratio $R(Q^2)$ then emerges naturally in chiral soliton models as it basically stems from the isospin being generated from a rigid rotation in flavor space. In any event, we are mainly interested in whether or not the two–photon exchange coupled via the anomaly significantly contributes to the Rosenbluth cross section. To answer this question qualitatively, no further fine tuning of the model to reproduce the from factors in detail is required.

As will be shown in the next chapter, only the form factor F_A contributes to the interference with the one–photon exchange. For its computation in the Breit frame we consider the spatial components of W^μ in eqs (3.3) and (3.4),

$$\langle N(\vec{p}')|W_i|N(\vec{p})\rangle = \pm\frac{1}{9\pi M}\chi'^\dagger \left[H_0(Q^2)\sigma_i + H_2(Q^2)\left(\sigma_i - 3\hat{q}_i\hat{q}\cdot\vec{\sigma}\right)\right]\chi\,. \qquad (4.11)$$

Here χ refers to the two–component nucleon spinor. Doting this matrix element into $\hat{q}$ as well as averaging the $\vec{q}$ directions yields two relations between H_i and the form factors in eq. (4.5) from which

$$F_A(Q^2) = \pm\frac{1}{18\pi ME}\left[H_0(Q^2) + H_2(Q^2)\right] \qquad (4.12)$$

is extracted. The two signs refer to proton and nucleon, respectively. In the next step we compute the left hand side of eq. (4.11) in the soliton model with the techniques of ref. [25]: We substitute the rotating hedgehog configuration, eq. (2.4) into the expression for W_i that we extracted from eqs (3.3) and (3.4) and take matrix elements between nucleon states. They elements are straightforwardly evaluated with the help of eq. (2.8) and by noting that $A^\dagger\hat{Q}A = \frac{1}{6}\mathbb{1} + \frac{1}{2}D_{3i}\tau_i$. Finally we encounter the Fourier transforms of the chiral angle in the form

$$
\begin{aligned}
H_0(Q^2) &= M^2\int_0^\infty dr r^2 \left[\frac{dF}{dr} + \frac{2}{r}\sin F\cos F\right] j_0(|\vec{q}|r) \\
H_2(Q^2) &= M^2\int_0^\infty dr r^2 \left[\frac{dF}{dr} - \frac{1}{r}\sin F\cos F\right] j_2(|\vec{q}|r)\,,
\end{aligned}
\qquad (4.13)
$$

where $j_\ell(z)$ denotes the spherical Bessel functions associated with orbital angular momentum ℓ. Once these momentum dependent functions are computed they are subject to the boost transformation, eq. (4.8) with $n_{\mathrm{WZ}} = 2$. The resulting form factors H_0 and H_2 are displayed in figure 7.

As long as we omit time derivatives of the collective coordinates, the spin operator, eq. (2.5) does not explicitly enter. In any event, it can only occur in W_0 which is the only component that contains a time derivative. Direct evaluation of $\langle W_0\rangle$ gives zero for this nucleon matrix element after hermitionizing eventual ordering ambiguities.
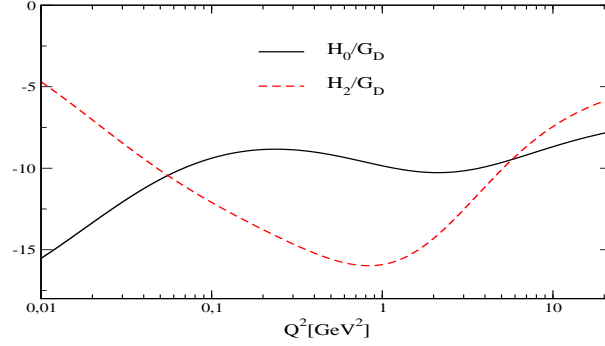
FIG. 7: Nucleon axial form factors that contribute at the level of the two–photon exchange to the elastic electron nucleon scattering. They are computed from eq. (4.13) with the boost, eq. (4.8) applied with $n_{\mathrm{WZ}} = 2$ and normalized to the dipole form eq. (4.9). Again we adopted $e_{\mathrm{Sk}} = 3.8$.

V. RESULTS

We mainly intend to point out that there is an effect of the anomaly that reveals itself as relevant two–photon contributions to electron nucleon scattering processes. Hence we do not attempt any fine tuning of parameters.

To estimate this effect we merely have to substitute the matrix element of W_μ in the form factor decomposition, eq. (4.5) into the Feynman diagrams of figure 3. We may then formally write the corresponding matrix element for the electron nucleon scattering as

$$iM_{2\gamma}^{\mathrm{WZ}}(q^2) = -i\alpha^2 \overline{u}(k') \left[w_1(q^2) k'^\mu \gamma_5 + w_2(q^2) q^\mu \gamma_5 + w_3(q^2) \gamma^\mu \gamma_5 \right] u(k)$$

$$\times \overline{U}(\vec{p}') \left[\gamma_\mu F_A(Q^2) + q_\mu F_p(Q^2) + i\sigma_{\mu\nu} q^\nu F_E(Q^2) \right] \gamma_5 \, U(\vec{p}) . \quad (5.1)$$

Again q_μ is the momentum transferred from the electrons (represented by the spinors $u(k)$ and $u(k')$) to the protons via the two photons. The above parameterization is general for couplings via axial currents that enter here because of the ϵ–tensor in the Wess–Zumino term [9]. Henceforth we will no longer make explicit the dependence on the momentum transfer $q^2 = -Q^2$, which is negative for this scattering process.

The effects of the photon–electron loop are contained in the form factors $w_i(q^2)$. We will discuss the relevant pieces thereof later. We are mainly interested in the (unpolarized) interference with the one photon exchange whose transition matrix element is given by the electro–magnetic nucleon form factors, *cf.* eq. (4.1),

$$iM_\gamma = i\frac{4\pi\alpha}{q^2} \overline{u}(k') \gamma^\mu u(k) \overline{U}(\vec{p}') \left[\gamma_\mu F_1(Q^2) + \frac{i\sigma_{\mu\nu} q^\nu}{2M} F_2(Q^2) \right] U(\vec{p})$$

$$= i\frac{4\pi\alpha}{q^2} \overline{u}(k') \gamma^\mu u(k) \overline{U}(\vec{p}') \left[\gamma_\mu G_M(Q^2) - \frac{1}{2M} \left(p_\mu + p'_\mu \right) F_2(Q^2) \right] U(\vec{p}) , \quad (5.2)$$

where in the second equation we employed the Gordon decomposition. We sum the interference contributions over electron and proton spins. This computation is significantly simplified by using of momentum conservation and the fact that the spinors $U(\vec{p})$ and $u(\vec{k})$ obey free Dirac equations. Only a few structures contribute when we average over polarizations.

The intrinsic parity of γ_5 requires four additional γ matrices under the Dirac sum. Two of which stem from $U(p)\overline{U}(p) = (\not{p}+m)/2$ and the equivalent construction from p'. A third one comes from the γ_μ in the one photon exchange, eq. (5.2). Hence the forth must originate from the from factor decomposition in eq. (5.1). This directly shows that the contribution from the one–photon exchange to the interference is linear in the magnetic form factor G_M. Since we also have a Gordon–type decomposition $\overline{U}(p')\sigma_{\mu\nu}q^\nu\gamma_5 U(p) = i\overline{U}(p')\left(p_\mu + p'_\mu\right)\gamma_5 U(p)$ the Dirac structures associated with neither F_p nor F_E satisfy this criterion. A similar argument, of course, holds for the electron form factors w_1 and w_2. Finally, the intrinsic parity of the ϵ–tensor enforces the sum over polarizations to be antisymmetric under $p \leftrightarrow p'$ (or, equivalently $k \leftrightarrow k'$). Up to overall constants, these considerations determine the final result

$$\sum_{\text{spins}} M_\gamma^* M_{2\gamma}^{\text{WZ}} = \frac{128\pi\alpha^3}{q^2} w_3 F_A G_M \left[(k \cdot p')^2 - (k \cdot p)^2\right]$$

$$= 128\pi\alpha^3 \, w_3 F_A G_M M^2 \sqrt{\tau\left(1+\tau\right)\frac{1+\epsilon}{1-\epsilon}} \tag{5.3}$$

that formally shows a deviation from the linear ϵ–dependence found in the one–photon exchange approximation, eq. (1.3). We have written this equation such as to make explicit the dependence on $\sqrt{(1-\epsilon)/(1+\epsilon)}$ as required by general properties and consistency conditions for the two–photon interaction [9].

If W_μ were a total derivative, F_p would be the only non–zero from factor and thus the interference would vanish in the limit $m_e \to 0$. On the other hand, the q_μ term of the hadron form factor characterizes the $\pi^0 \to e^- e^+$ decay that we discussed earlier.

The information about the photon loop is contained in the electron form factor that we compute in dimensional regularization,

$$w_3 = -2 - \int_0^1 dy \int_0^{1-y} dx \, \frac{(1-x)\,q^2}{x^2 m_e^2 - (1-x-y)\,yq^2 - i\epsilon}$$
$$+6 \int_0^1 dy \int_0^{1-y} dx \left[\frac{4}{4-D} - \ln\left(\frac{x^2 m_e^2 - (1-x-y)\,yq^2}{4\pi\Lambda^2}\right)\right] - \frac{\chi(\Lambda)}{2}. \tag{5.4}$$

We have made explicit the contribution from the counterterm, eq. (3.4) that eventually cancels the part that diverges as $D \to 4$, according to eq. (3.5) . It is interesting to consider the leading contribution in the limit of vanishing electron mass,

$$w_3 \xrightarrow[m_e \to 0]{} \widetilde{w}_3 = -2\ln\left(\frac{m_e^2}{Q^2}\right) + 7 + \frac{1}{2}\chi_{\text{fin}}(\Lambda) - 3\ln\left(\frac{Q^2}{\Lambda^2}\right) \tag{5.5}$$

and compare it with eq. (3.7). First, we notice that the Λ–dependence is the same, so that after fixing the counterterm via the decay $\pi \to e^- e^+$ the model prediction for the unpolarized cross section does not possess any renormalization scale dependence. Second, the $m_e \to 0$ singularity is more severe for the decay than for the considered cross section. This reflects the fact that the $\left[\ln\left(\frac{m_e^2}{m_\pi^2}\right)\right]^2$ divergence is buried[2] in the electron form factors w_1

---

[2] In general the denominator in the first integral in eq. (5.4) always yields a double logarithm as the leading divergence. However, for the special combination $1 - x$ in numerator of the first integral in eq. (5.4) this piece drops out.

and w_2 that do not contribute to the cross section after averaging the polarizations. In turn this implies that for a prescribed amplitude A in eq. (3.7), $\chi_{\mathrm{fin}} = \mathcal{O}\left[\ln m_e^2\right]^2$. Hence, for momenta $Q^2 \gg m_e^2$ the counterterm would actually dominate this contribution to the cross section if we chose such a renormalization condition[3]. The discussion of this singularity in ref. [22] suggests that it arises independently of the high momentum treatment. In ref. [23] the authors carefully analyze the (double)–logarithmic singularities in the box diagrams of figure 2. In that case, single logarithmic singularities emerge always while double logarithmic singularities only occur when the momentum transfer roughly equals the mass of the exchanged hadronic resoncance. The triangle diagrams (figure 3) do not contain hadronic resonances. Thus the non–existence of double logarithmic singularities in their contribution to electron nucleon scattering is expected; even though they may generally emerge as the rare π^0 decay exemplifies.

To facilitate the discussion of our numerical results for the two–photon exchange contribution from the Wess–Zumino term we identify the tree level cross–section, eq. (1.3) and introduce the reduced cross–section,

$$\left(\frac{d\sigma}{d\Omega}\right)_R = \frac{\epsilon}{\tau}\left(1+\tau\right)\frac{d\sigma}{d\Omega}\bigg/\left(\frac{d\sigma}{d\Omega}\right)_{\mathrm{Mott}}, \tag{5.6}$$

so that

$$\begin{aligned}
\left(\frac{d\sigma}{d\Omega}\right)_R &= G_M^2 + \frac{\epsilon}{\tau}G_E^2 + \frac{2\alpha}{\pi}\widetilde{w}_3 M^2 F_A G_M \sqrt{\tau(1+\tau)(1-\epsilon^2)} \\
&= \frac{G_M^2}{\tau}\left[\tau + \epsilon\frac{G_E^2}{G_M^2} + \frac{2\alpha}{\pi}\widetilde{w}_3 M^2 \frac{F_A}{G_M}\sqrt{\tau^3(1+\tau)(1-\epsilon^2)}\right].
\end{aligned} \tag{5.7}$$

For small ϵ the predicted correction to the Rosenbluth form is $\mathcal{O}(\epsilon^2)$ and thus small. Note, that in the form of the second equation the ambiguities in choosing the powers n_X, cf. eq. (4.8) cancel within the square bracket.

In figures 8 and 9 we present our result for $\left(\frac{d\sigma}{d\Omega}\right)_R$. To mitigate the model deficiencies associated with G_M we compare the model prediction

$$r_{\mathrm{mod}}(\epsilon) = \frac{1 + \frac{\epsilon}{\tau}\frac{G_E^2}{G_M^2} + \frac{2\alpha}{\pi}\widetilde{w}_3 M^2 \frac{F_A}{G_M}\sqrt{\tau(1+\tau)(1-\epsilon^2)}}{1 + \frac{2\alpha}{\pi}\widetilde{w}_3 M^2 \frac{F_A}{G_M}\sqrt{\tau(1+\tau)}} \tag{5.8}$$

to the ratio of empirical data

$$r_{\mathrm{exp}}(\epsilon) = \frac{(d\sigma(\tau,\epsilon)/d\Omega)_R}{(d\sigma(\tau,0)/d\Omega)_R}. \tag{5.9}$$

By construction, the experimental value $(d\sigma(\tau,0)/d\Omega)_R$ is the magnetic form factor as obtained from the Rosenbluth method. We recognize from these figures that the additions from the Wess–Zumino term to the unpolarized cross section work into the direction required by the data. However, they are about a factor five too small for low Q^2. For larger Q^2 it may

---

[3] In a fully renormalizable theory renormalization conditions are commonly imposed on Green's functions with external legs amputated. This would translate to constrain the off–shell amplitude A rather than the physical on–shell decay width Γ via a renormalization condition.
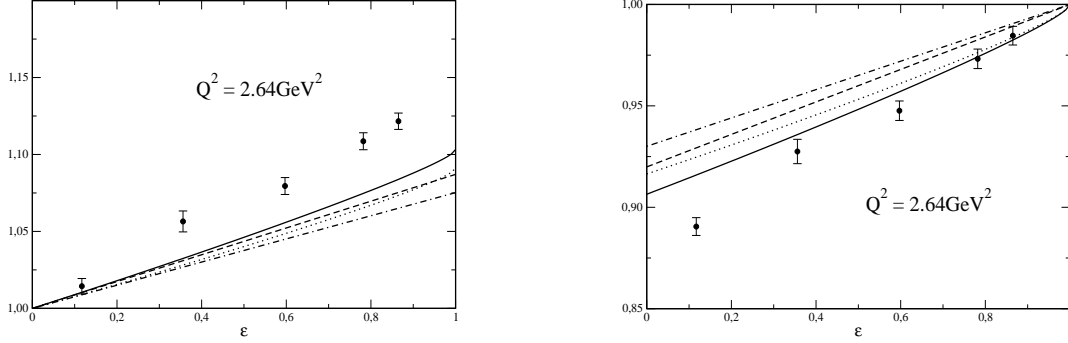
FIG. 8: Results for the normalized reduced cross section, eq. (5.8), compared to experimental data [42]. The full line is our model result, the dashed line is the model result at the one–photon exchange level, *i.e.* $F_A \equiv 0$. The dotted and dashed–dotted lines are similarly obtained with the polarization result for G_E/G_M, eq. (1.5) substituted for the second term of the numerator in eq. (5.8). The left and right panels distinguish the normalization at $\epsilon = 0$ and $\epsilon = 1$, respectively.
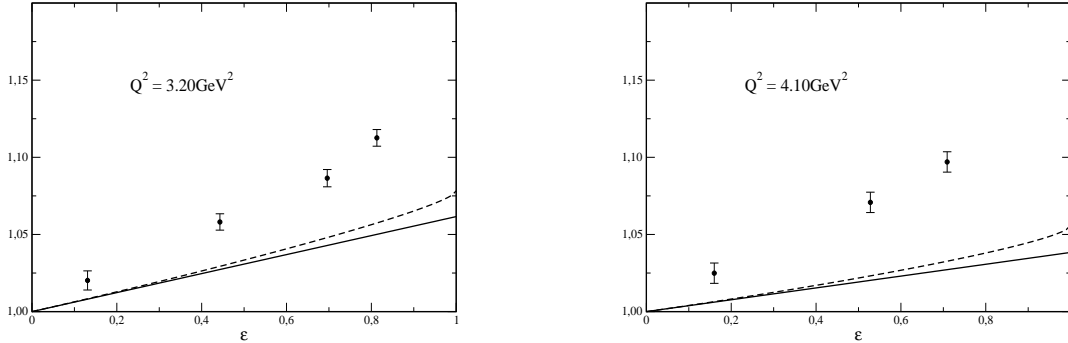

FIG. 9: Same as the left panel of figure 8 for two different values of Q^2.

fall short by an order of magnitude. When we normalize with respect to $\epsilon = 0$ these additions are strongest around the end–point $\epsilon \to 1$. One the other hand, this normalization point is not very special and we may adopt equally well $\epsilon = 1$, as displayed in the right panel of figure 8. In that case the agreement with data occurs to be significantly better, yet it is merely a matter of presentation. It also suggests that this two–photon effect would be most strongly pronounced around $\epsilon \approx 0$. This is, of course, not the case as can easily be recognized by inspecting eq. (5.3). However, a common procedure in the literature, that discusses the two–photon contamination in terms of the quantity δ defined via

$$\left(\frac{d\sigma}{d\Omega}\right)_R = \left[G_M^2 + \frac{\epsilon}{\tau}G_E^2\right](1+\delta) \tag{5.10}$$

and that we show in figure 10, suggests otherwise because of the ϵ dependence of the pre–factor. Nevertheless such a presentation is interesting as it disentangles the two–photon exchange contribution, *i.e.* the last term in eq. (5.7) normalized to the one–photon contribution to the cross section. Experimentally this corresponds to the ratio of the difference and the sum of the cross sections for unpolarized electron–proton and positron–proton scattering. There are no new data on this separation. However, the existing data [43, 44] indicate that δ should be negative [12].
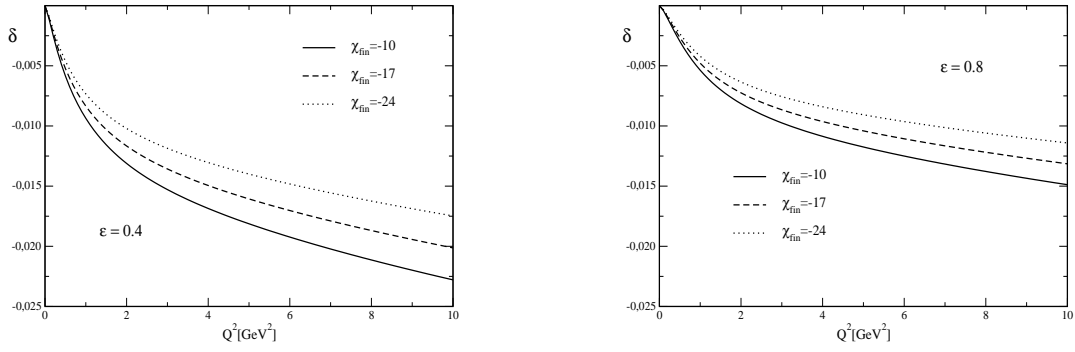
FIG. 10: The two–photon exchange contribution, δ in eq. (5.10) for two values of the photon polarization parameter ϵ as a function of the momentum transfer Q^2. Also given are the results for different finite parts of the counterterm coefficient, eq. (3.5).
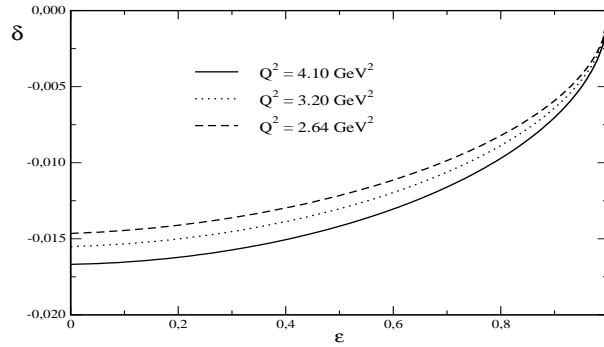

FIG. 11: The model prediction for the two–photon exchange contribution, δ as a function of the photon polarization parameter ϵ.

We observe that the anomaly contribution to δ has a large slope at small momentum transfer, Q^2 while it levels off with increasing Q^2. This dependence is uniform as we vary ϵ. As a function of ϵ with fixed Q^2 we find the largest slope of δ around $\epsilon \sim 1$, as shown in figure 11. These features are quite different from the contributions of the box diagrams (figure 2) that were estimated in ref. [12] outside of any soliton model. We stress that this is not a contradiction, rather the opposite is the case because these results must be added in a full computation of the two–photon effects onto the Rosenbluth method.

After eq. (3.8) we argued that we set the renormalization scale $\Lambda = 1\text{GeV}$ and considered three cases $\chi_{\text{fin}}(\Lambda) = -24, -17, -10$ that are suggested by the data for the decay $\pi^0 \to e^- e^+$. We display the corresponding variations for the cross section in figure 10. This uncertainty translates into an 10–20% effect for the two–photon contribution to the cross section. These minor variations with the uncertainty in the fixing the model parameter from the underlying process $\pi^0 \to e^+ e^-$ is reassuring as it shows that the $\ln m_e^2$ effects are not as severe as suspected. All results shown in figures 8 and 9 refer to the central value $\chi_{\text{fin}}(\Lambda) = -17$.

We have also investigated the non–anomalous two–photon vertex that originates from the non–linear σ–model, eq. (4.3). Since this interaction does not have any derivative operator, the corresponding triangle diagram is ultra–violet finite and thus no counterterm is required. Yet we find that the corresponding matrix element, $M_{2\gamma}^{\text{nl}\sigma}$ vanishes as $m_e \to 0$. Hence this

interaction gives negligible contribution within the Rosenbluth method, if at all.

VI. CONCLUSION

We have performed a model calculation to shed some light on the discrepancies that arise from different methods to extract the nucleon electro–magnetic form factors from data. These discrepancies are assumed to be resolved by the inclusion of two–photon processes in the computation of electron–proton reactions. Here we have focused on the contribution of such a process with the least model dependence and fewest assumptions about off–shell form factors. This appears to be the anomaly induced two–photon vertex because it actually is a QCD property. It naturally emerges from the nucleon pion cloud coupling to the QCD anomaly. This particular two–photon exchange contribution to the elastic electron nucleon scattering has previously been overlooked presumably because it vanishes in the one–pion exchange approximation. However there is no reason for it to be particularly small beyond that approximation. For these reasons we focus on this particular process, which of course does not fully explain the observed discrepancies by itself. Nevertheless, it is interesting to investigate this effect by its own as it has not been considered previously in the context of electron nucleon scattering. Of course, there is no reason to assume that this piece by itself fully resolves the discrepancy between the Rosenbluth and polarization analyses. At face value the corresponding Feynman diagram is ultra–violet divergent and requires renormalization. We impose a renormalization condition that reproduces the empirical decay width for the process $\pi^0 \to \gamma\gamma$. This is an *ad hoc* attempt to deal with the (unknown) off–shell behavior of the anomalous $\pi^0 \to \gamma\gamma$ interaction that has been successfully utilized for the description of the pion decay. The Skyrme soliton model is a perfect and the simplest tool to study this anomalous contribution to electron proton scattering because it provides both, the pion cloud picture of the nucleon and a unique description of the pion anomaly coupling via the Wess–Zumino term. We do not exclude that more sophisticated models might provide more reliable estimates of this effect.

The so–computed anomaly contribution to the unpolarized cross section has a minor effect on the cross section, of the order of a few per cent. This is to be anticipated for an order $\alpha = 1/137$ contamination. Even though this contribution corrects the leading order result into the proper direction these corrections are not sufficient to fully explain the observed discrepancy. In this context we stress that this anomaly contribution must be considered in addition to contributions from the box diagrams in figure 2. Unfortunately, their computation is quite model dependent thereby leading to quite some uncertainties, in particular at large momentum transfers. Eventually they can be reduced somewhat by phenomenological input for the generalized parton distributions from the amplitude of deeply virtual Compton scattering [45]. The studies of ref. [12] indicate that these box diagrams are the most significant for δ (the two–photon piece in the unpolarized cross section) at small ϵ. The anomaly contribution that we have computed enhances δ at moderate ϵ so that we expect a negative, say about 5%, effect at small and moderate ϵ while at the boundary $\epsilon \to 1$ the contributions of both, the anomaly and the box diagrams are compatible with zero.

In general the model contains additional triangle diagram (non–anomalous) type two–photon processes like those shown in figure 3 where the two photons couple simultaneously to the pion cloud of the nucleon. In the present model it is natural to assume that the dominant such process stems from the non–linear σ model. We have seen that it vanishes

as the momentum transfer is large compared to the electron mass.

In the next step we will have to investigate the anomaly contribution in the framework of the polarization method. In particular the effects of the form factors F_E and F_p, that do not show up in the Rosenbluth method, will be of future interest.

Acknowledgments

---

[1] G. Höhler *et al.*, Nucl. Phys. B **114** (1976) 505.
R. C. Walker *et al.*, Phys. Rev. D **49** (1994) 5671.
L. Andivahis *et al.*, Phys. Rev. D **50** (1994) 5491.

[2] M. K. Jones *et al.* [Jefferson Lab Hall A Collaboration], Phys. Rev. Lett. **84** (2000) 1398. [arXiv:nucl-ex/9910005].
O. Gayou *et al.* [Jefferson Lab Hall A Collaboration], Phys. Rev. Lett. **88** (2002) 092301. [arXiv:nucl-ex/0111010].
V. Punjabi *et al.*, Phys. Rev. C **71** (2005) 055202 [Erratum-ibid. C **71** (2005) 069902] [arXiv:nucl-ex/0501018].

[3] F. Iachello, A. D. Jackson and A. Lande, Phys. Lett. B **43** (1973) 191.

[4] G. Holzwarth, PiN Newslett. **10** (1995) 103 [arXiv:hep-ph/9507360]; Z. Phys. A **356** (1996) 339 [arXiv:hep-ph/9606336].

[5] M. E. Christy *et al.* [E94110 Collaboration], Phys. Rev. C **70** (2004) 015206 [arXiv:nucl-ex/0401030].
I. A. Qattan *et al.*, Phys. Rev. Lett. **94** (2005) 142301 [arXiv:nucl-ex/0410010].

[6] E. Tomasi-Gustafsson and G. I. Gakh, Phys. Rev. C **72** (2005) 015209 [arXiv:hep-ph/0412137].
V. Tvaskis *et al.*, Phys. Rev. C **73** (2006) 025206 [arXiv:nucl-ex/0511021].

[7] J. Arrington, Phys. Rev. C **68** (2003) 034325 [arXiv:nucl-ex/0305009]; Phys. Rev. C **69** (2004) 022201 [arXiv:nucl-ex/0309011]; Phys. Rev. C **71** (2005) 015202 [arXiv:hep-ph/0408261].
H. Gao, Int. J. Mod. Phys. A **20** (2005) 1595.

[8] P. A. M. Guichon and M. Vanderhaeghen, Phys. Rev. Lett. **91** (2003) 142303 [arXiv:hep-ph/0306007].

[9] M. P. Rekalo and E. Tomasi-Gustafsson, Eur. Phys. J. A **22** (2004) 331 [arXiv:nucl-th/0307066]; Nucl. Phys. A **742** (2004) 322 [arXiv:nucl-th/0402004].

[10] Y. C. Chen, C. W. Kao and S. N. Yang, Phys. Lett. B **652** (2007) 269 [arXiv:nucl-th/0703017].

[11] C. E. Carlson and M. Vanderhaeghen, Annu. Rev. Nucl. Part. Sci. **57** (2007) 171, [arXiv:hep-ph/0701272]

[12] P. G. Blunden, W. Melnitchouk and J. A. Tjon, Phys. Rev. C **72** (2005) 034612 [arXiv:nucl-th/0506039].

[13] P. Jain, S. D. Joglekar and S. Mitra, Eur. Phys. J. C **52** (2007) 339 [arXiv:hep-ph/0606149].

[14] J. Arrington, W. Melnitchouk and J. A. Tjon, Phys. Rev. C **76** (2007) 035205 [arXiv:0707.1861 [nucl-ex]].

[15] S. Kondratyuk and P. G. Blunden, Phys. Rev. C **75** (2007) 038201 [arXiv:nucl-th/0701003].

[16] C. F. Perdrisat, V. Punjabi and M. Vanderhaeghen, Prog. Part. Nucl. Phys. **59** (2007) 694 [arXiv:hep-ph/0612014].

[17] H. Weigel, Lect. Notes Phys. **743** (2008) 1.

[18] B. Schwesinger, Phys. Lett. B **298** (1993) 17.
C. Gobbi, C. L. Schat and N. N. Scoccola, Nucl. Phys. A **598** (1996) 318 [arXiv:hep-ph/9509211].
F. Meier and H. Walliser, Phys. Rept. **289** (1997) 383 [arXiv:hep-ph/9602359].
N. N. Scoccola, H. Weigel and B. Schwesinger, Phys. Lett. B **389** (1996) 433 [arXiv:hep-ph/9608395].

[19] E. Witten, *Nucl. Phys.* **B223** (1983) 422, 433.

[20] O. Kaymakcalan, S. Rajeev and J. Schechter, Phys. Rev. D **30** (1984) 594.

[21] M. J. Savage, M. E. Luke and M. B. Wise, Phys. Lett. B **291** (1992) 481 [arXiv:hep-ph/9207233].

[22] L. Bergstrom, Z. Phys. C **14** (1982) 129.
A. E. Dorokhov and M. A. Ivanov, Phys. Rev. D **75** (2007) 114007 [arXiv:0704.3498 [hep-ph]].

[23] A. V. Afanasev and N. P. Merenkov, Phys. Rev. D **70** (2004) 073002 [arXiv:hep-ph/0406127]; Phys. Lett. B **599** (2004) 48 [arXiv:hep-ph/0407167].

[24] W. M. Yao *et al.* [Particle Data Group], J. Phys. G **33** (2006) 1.

[25] E. Braaten, S. M. Tse and C. Willcox, Phys. Rev. D **34** (1986) 1482.

[26] X. D. Ji, Phys. Lett. B **254** (1991) 456.

[27] B. D. Milbrath *et al.* [Bates FPP collaboration], Phys. Rev. Lett. **80**, 452 (1998) [Erratum-ibid. **82**, 2221 (1999)] [arXiv:nucl-ex/9712006].

[28] M. K. Jones *et al.* [Jefferson Lab Hall A Collaboration], Phys. Rev. Lett. **84** (2000) 1398 [arXiv:nucl-ex/9910005].

[29] T. Pospischil *et al.* [A1 Collaboration], Eur. Phys. J. A **12**, 125 (2001).

[30] O. Gayou *et al.*, Phys. Rev. C **64**, 038202 (2001).

[31] O. Gayou *et al.* [Jefferson Lab Hall A Collaboration], Phys. Rev. Lett. **88** (2002) 092301 [arXiv:nucl-ex/0111010].

[32] V. Punjabi *et al.*, Phys. Rev. C **71**, 055202 (2005) [Erratum-ibid. C **71**, 069902 (2005)] [arXiv:nucl-ex/0501018].

[33] M. K. Jones *et al.* [Resonance Spin Structure Collaboration], Phys. Rev. C **74** (2006) 035201 [arXiv:nucl-ex/0606015].

[34] C. B. Crawford *et al.*, Phys. Rev. Lett. **98** (2007) 052301 [arXiv:nucl-ex/0609007].

[35] G. Ron *et al.*, Phys. Rev. Lett. **99** (2007) 202002 [arXiv:0706.0128 [nucl-ex]].

[36] J. Gasser and H. Leutwyler, Nucl. Phys. B **250** (1985) 465.

[37] Ulf–G. Meißner, AIP Conf. Proc. **904**, 142 (2007) [arXiv:nucl-th/0701094].

[38] B. Schwesinger, H. Weigel, G. Holzwarth and A. Hayashi, Phys. Rept. **173** (1989) 173.

[39] G. Holzwarth, arXiv:hep-ph/0511194.

[40] A. N. Mitra and I. Kumari, Phys. Rev. D **15** (1977) 261.

[41] J. J. Kelly, Phys. Rev. C **66** (2002) 065203 [arXiv:hep-ph/0204239].

[42] I. A. Qattan *et al.* in ref. [5].

[43] A. Browman, F. Lui, and C. Schaerf, Phys. Rev. **139** (1965) B1079.

[44] J. Mar *et al.*, Phys. Rev. Lett. **21** (1968) 482.

[45] Y. C. Chen *et al.*, Phys. Rev. Lett. **93** (2004) 122301 [arXiv:hep-ph/0403058].
A. V. Afanasev *et al.*, Phys. Rev. D **72** (2005) 013008 [arXiv:hep-ph/0502013].